International Journal of Heat and Mass Transfer 129 (2019) 103–112

Contents lists available at ScienceDirect

International Journal of Heat and Mass Transfer

journal homepage: www.elsevier.com/locate/ijhmt

Experimental study of forced convective heat transfer in grille-particle composite packed beds

Yingxue Hu [a], Jingyu Wang [a], Jian Yang [a,b,*], Issam Mudawar [b], Qiuwang Wang [a]

[a] Key Laboratory of Thermo-Fluid Science and Engineering, Ministry of Education, School of Energy and Power Engineering, Xi'an Jiaotong University, Xi'an, Shaanxi 710049, PR China
[b] Purdue University Boiling and Two-Phase Flow Laboratory (PU-BTPFL), School of Mechanical Engineering, 585 Purdue Mall, West Lafayette, IN 47907, USA

ARTICLE INFO

Article history:
Received 7 August 2018
Received in revised form 15 September 2018
Accepted 20 September 2018
Available online 25 October 2018

Keywords:
Packed bed
Grille-particle composite packing
Random packing
Forced convective heat transfer
Pressure drop
Heat transfer efficiency

ABSTRACT

Due to high surface area-to-volume ratio and superior thermal performance, packed beds are widely used in variety of industries. In the present study, forced convective heat transfer in a novel grille-particle composite packing (GPCP) bed, was experimentally investigated in pursuit of reduced pressure drop and enhanced overall heat transfer. The effects of sub-channel to particle diameter ratio, grille thickness and grille thermal conductivity on pressure drop, Nusselt number and overall heat transfer efficiency in the grille-particle channel were carefully analyzed. And performances of grille-particle channels were compared with those of random particle channels in detail. It is shown that looser packing structure compromises heat transfer in the grille-particle channel, while decreasing pressure drop and improving overall heat transfer efficiency. Meanwhile, for the same Reynolds number and particle diameter, higher grille thermal conductivity and thinner grille thickness also improve overall heat transfer performance. Finally, when compared with random packing, both pressure drop and heat transfer in grille-particle channels are shown to be reduced, while overall heat transfer efficiency is improved, especially when employing relatively small particle diameters.

1. Introduction

Due to high surface area-to-volume ratio and advantageous internal structure, porous media have been shown to greatly improve heat transfer performance [1]. Packed beds represent an important application of porous media, and are widely used in chemical catalytic reactors, absorption towers, high temperature gas cooled nuclear reactors, electrical cooling devices, and numerous other applications [2–6].

Understanding the internal fluid flow and heat transfer characteristics is of paramount importance to the design of packed beds, evidenced by findings from numerous prior studies. For example, Jiang et al. [7] conducted experiments involving forced convective heat transfer in plate channels filled with glass or metallic particles. Their results showed a 5–12 fold enhancement in local heat transfer coefficient when compared with a particle-free channel. They also showed that a sintered particle bed performed better than a smooth particle bed [8]. Jeng et al. [9] investigated an asymmetrically heated channel filled with brass beads with different diameters. Their results point to particle diameter as a suitable parameter for generalized heat transfer characterization of packed beds. In their naphthalene sublimation mass transfer experiments, Ahmadi Motlagh and Hashemabadi [10] investigated heat transfer behavior in a randomly packed bed filled with cylindrical particles. Meanwhile, several investigations were focused on local flow and heat transfer characteristics within the packed channels, which contributed to improved understanding of transport behavior inside packed pores. For example, Dixon et al. [11] investigated radial temperature distributions in randomly packed beds of spheres both experimentally and numerically. Freund et al. [12] showed a strong dependence of not only local behavior but also integral quantities like pressure drop on local pore structure in a fixed bed with $D/d_p = 3$. Nijemeisland and Dixon [13] proposed a relationship between local flow pattern and local wall heat flux for a randomly packed bed with $D/d_p = 4$. Baker and Tabor [14] used CFD to investigate transitional air flow in a packed bed of 160 spheres with Monte Carlo packing ($D/d_p = 7.14$). Eppinger et al. [15] developed an improved meshing method for spherical fixed beds, which was proved quite effective at capturing internal distributions of porosity and pressure drop. Their study encompassed CFD investigation of laminar, transitional and turbulent flow in a packed bed with $3 < D/d_p < 10$.

* Corresponding author at: Key Laboratory of Thermo-Fluid Science and Engineering, Ministry of Education, School of Energy and Power Engineering, Xi'an Jiaotong University, Xi'an, Shaanxi 710049, PR China.
E-mail address: yangjian81@mail.xjtu.edu.cn (J. Yang).

https://doi.org/10.1016/j.ijheatmasstransfer.2018.09.103
0017-9310/

Nomenclature

A_{cross}	cross-sectional area of empty channel, m^2
A_g	area of grille, m^2
A_{heat}	area of heated channel wall, m^2
A_p	total surface area of particles in entire channel or sub-channel, m^2
A_{total}	total area of solid surfaces in test channel, m^2
d_h	hydraulic diameter of sub-channel, m
d_p	particle diameter, m
D	tube diameter, m
D_h	hydraulic diameter of empty channel, m
f_v	friction factor
h_{wf}	wall-to-fluid heat transfer coefficient, $W/(m^2 \cdot K)$
I	input current, A
L	length of test channel, m
N	tube to particle diameter ratio, sub-channel to particle diameter ratio
N_p	particle number
Nu_{wf}	wall-to-fluid Nusselt number
P_{cross}	cross section perimeter of empty channel, m
Pr	Prandtl number
q_w	heat flux of test channel, W/m^2
Q_{loss}	heat loss, W
Q_{total}	total heat, W
Re_D	superficial Reynolds number
Re_p	particle Reynolds number
T	temperature, K
T_{wx}	local temperature of channel wall, K
U	input voltage, V
v_{in}	inlet fluid velocity, m/s
V	volume of entire channel or sub-channel, m^3
V_p	total volume of particles in entire channel or sub-channel, m^3

Greek symbols

γ	overall heat transfer efficiency, $W/(m^2 \cdot K \cdot Pa)$
δ_g	thickness of grille, m
δ_w	distance from groove bottom to inner surface of test channel, m
ε	porosity
λ	thermal conductivity, $W/(m \cdot K)$
μ	dynamic viscosity, Pa·s
ρ	density, kg/m^3

Subscripts

cross	cross section
f	fluid
g	grille
in	inlet
out	outlet
p	particle
w	channel wall
∞	atmosphere

However, all above studies were limited to randomly packed beds, within which both fluid flow and heat transfer are inhomogeneous, and non-uniform distribution of void fraction renders hot spots hard to predict [16]. To tackle these shortcomings of random beds, Yang et al. [17,18] proposed several novel structured packed bed configurations. They investigated the effects of Reynolds number, packing form and particle shape on overall heat transfer efficiency both experimentally and numerically. They found these novel structures could both significantly reduce pressure drop and improve overall heat transfer efficiency. In a numerical study involving implementation of pebble-bed nuclear reactor (PBMR) in high temperature gas-cooled reactors [19], ordered particle arrangements, like simple cubic (SC), body-centered cubic (BCC) and face-centered cubic (FCC), were found to yield different flow distributions within the packed bed. The SC arrangement formed a simple straight flow path so that most of the flow would pass without interaction. However, staggered particle arrangements were found to produce complex flow interactions.

A packed bed utilizing grille-particle composite packing (GPCP), which is the focus of the present study, was proposed by Strangio et al. [20], and its characteristics were explored in detail in later studies [21–24]. In GPCP, a specific framework is initially inserted into the channel to facilitate particle filling. In effect, the packed bed would be acquired a structure consisting of several sub-channels, wherein particles would be packed in either an ordered or disordered manner in each sub-channel. Calis et al. [21] and Romkes et al. [22] conducted numerical and experimental investigations of fluid flow and heat transfer, respectively, in a single GPCP sub-channel. It showed a substantial decrease in GPCP sub-channel pressure drop when compared with a random particle channel [21]. Recently, Wang et al. [23] investigated convective heat transfer in a GPCP channel containing 7×7 sub-channels. Their results proved that, the full packed bed with GPCP composite packing could promote significant enhancement in overall heat transfer efficiency when compared to both the full packed beds with random and SC packing. The same study provided detailed investigation of the effects of grille on hydrodynamic and heat transfer performances in terms of variations of flow and temperature distributions within, but didn't consider effects of grille conductivity. Motivated by the findings of Wang et al. [23], Hu et al. [24] examined numerically (using the Taguchi optimization method) the effects of graphite grille parameters on heat transfer performance for a high temperature gas cooled nuclear reactor. Their results showed that effects of sub-channel to particle diameter ratio (N) are more significant than those of grille thickness or thermal conductivity.

Based on the above studies, it can be concluded that GPCP has the potential to both reduce pressure drop and enhance overall heat transfer in packed beds. However, until recently, published GPCP studies have been focused mostly on heat transfer between particles and fluid, while heat transfer between channel wall and fluid remains virtually untouched. This deficiency is the primary impetus for the present paper. Here, forced convective heat transfer in GPCP will be investigated experimentally to assess the effects of sub-channel to particle diameter ratio, grille thickness and grille thermal conductivity on pressure drop, Nusselt number along the heated channel wall and overall heat transfer efficiency in the packed channel. Additionally, performances of GPCP channels will be compared with those of random particle channels.

2. Experimental setup

2.1. Experimental system and procedure

Shown in Fig. 1, the experimental setup constructed for the present study is comprised of four sub-systems: (1) air supply system, (2) heating system, (3) data acquisition system, and (4) main test

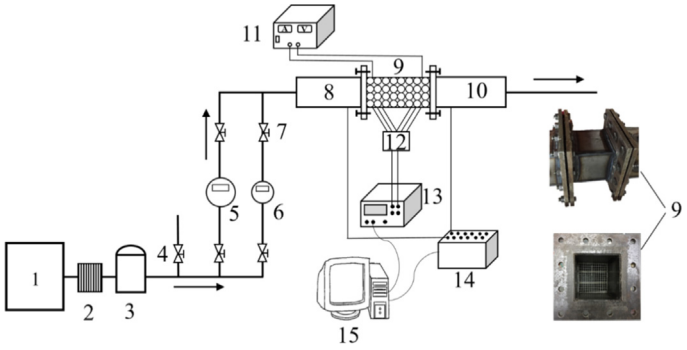

(1) compressor, (2) dryer, (3) tank, (4) bypass, (5, 6) vortex flowmeter, (7) valve, (8) inlet channel, (9) test channel, (10) outlet channel, (11) DC power, (12) multiplexer, (13) data acquisition, (14) pressure scanning valve, (15) computer.

Fig. 1. Experimental system.

section. The study employs air as working fluid, which is supplied by a screw compressor (Atlas Copco AP1600). Moisture is removed by a dryer before storing the air in the system's tank. The air flow rate is regulated with the aid of valves situated in two parallel branches, and flow rate is measured with the aid of one of two vortex flowmeters (8–55 m^3/h and 35–380 m^3/h). The flow then enters the inlet channel. This is followed by the test channel, which features a 100 mm × 100 mm cross-section and a length of 1000 mm (10 times the hydraulic diameter). The air then flows through the 100 mm × 100 mm × 500 mm outlet channel before it mixes with atmosphere.

The test channel receives constant heat flux along each channel wall, which is supplied by a DC-powered film heater. As shown in Fig. 2, the film heater is attached to the top surface of a 2.5 mm-thick brass plate, which serves as heat spreader. Both the film heater and brass plate have 100 mm × 100 mm area. The small gap between the cooper plate and outer surface of the test channel is filled with high conductivity thermal grease to minimize contact thermal resistance. The other side of the film heater is covered with approximately 60 mm-thick of glass cotton fiber to guard against heat loss to the ambient. A 10 mm-thick Bakelite plate is used to press the film heater and brass plate together. In order to contain particles in the test channel, two perforated stainless steel mesh screens are installed at the test channel's inlet and outlet. Between the inlet/outlet channels and the test channel, two pairs of rubber washers are installed to ensure leak proof seal and help prevent heat loss through the flanges.

Pressure in the test channel is measured with a pressure scanning valve (PSI 9100), and air temperature is measured with the aid of two type-K thermocouples located in the upstream and downstream sections, about 100 mm from the ends of test channel. As mentioned earlier, air flow rate is measured by one of two vortex flowmeters, and the heat flux (Q_{total}) controlled by a DC power source. As shown in Fig. 2, temperature distribution along the test channel wall is obtained by a series of eleven type-T thermocouples inserted each into a 100-mm long, 2-mm wide, and 1-mm deep grooves along the centerline of the channel wall. In order to get the accurate temperature distribution of the test channel wall, eleven long grooves were carved in the test channel's outside surface. Excellent thermocouple contact is achieved by filing the grooves with fuse material. A Keithelty 2700 system is used to acquire all signals from the facility's sensors, from which the data are stored in a personal computer.

2.2. Test section

The test channel is square in cross-section and fabricated from steel, and measures 2-mm thick, 100-mm wide and 120-mm long.

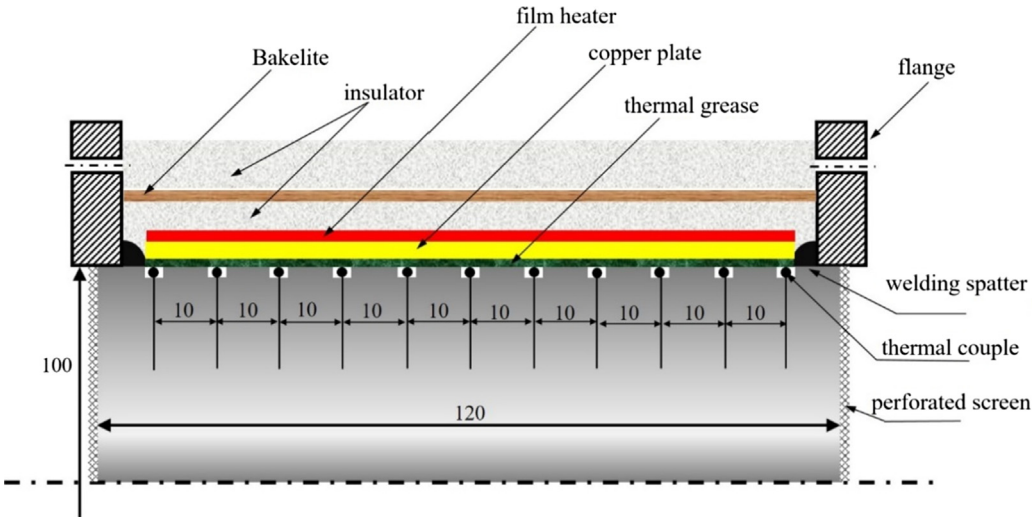

Fig. 2. Arrangement of thermocouples within the test section (unit: mm).

Both a random particle channel and a grille-particle channel are employed. Detailed geometrical parameters for all the packed channels tested are presented in Table 1, and photos of a random particle channel and several grille-particle channels are shown in Fig. 3.

2.3. Data reduction

The porosity (ε) of the packed bed (random particle channel or grille-particle channel) is calculated according to

$$\varepsilon = \frac{V - V_p}{V} \tag{1}$$

where V is the volume of the entire channel or a sub-channel and V_p the total volume of particles in the entire channel or a sub-channel.

Values of working parameters for the experiments performed in this study are presented in Table 2. The forced convective heat transfer characteristics of the test channel are estimated with the aid of several parameters, including superficial Reynolds number (Re_D) and wall-to-fluid Nusselt number (Nu_{wf}).

$$Re_D = \frac{\rho v_{in} D_h}{\mu} \tag{2}$$

$$h_{wf} = \frac{Q_{total} - Q_{loss}}{A_{heat}(T_w - T_f)} \tag{3}$$

$$Nu_{wf} = \frac{h_{wf} D_h}{\lambda_f} \tag{4}$$

$$D_h = \frac{4A_{cross}}{P_{cross}} \tag{5}$$

where v_{in} is average air velocity at the test channel inlet, ρ is air density, D_h is hydraulic diameter of an empty channel, Q_{total} and Q_{loss} are heat generated by the film heater and heat loss via the insulating layer, respectively, A_{heat} is area of the heated channel wall, T_w and T_f are average temperatures of the heated channel wall and fluid, respectively, and A_{cross} and P_{cross} are cross-sectional area and wetted perimeter of an empty channel, respectively.

The local temperature along the heated channel wall can be calculated as

Table 1
Ranges of geometrical and physical parameters for different packed channels tested.

	Packings	d_p (mm)	Grille material	δ_g (mm)	λ_g (W/m·K)	A_g ($\times 10^3 m^2$)	A_p ($\times 10^3 m^2$)	A_{total} ($\times 10^3 m^2$)
Particle channels	P1	6	–	–	–	–	730.6	778.6
	P2	9	–	–	–	–	480.2	528.2
	P3	12	–	–	–	–	355.6	403.6
Grille-particle channels	G1P1-Br	6	Brass	2.6	173	241.9	421.1	704.7
	G1P1-Al	6	Aluminum	2.6	155	241.9	424.7	708.3
	G1P1-St	6	Steel	2.6	60	241.9	423.5	707.1
	G2P1-St	6	Steel	0.5	60	322.6	559.0	929.6
	G1P2-Br	9	Brass	2.6	173	241.9	191.0	474.6
	G1P2-Al	9	Aluminum	2.6	155	241.9	189.9	473.5
	G1P2-St	9	Steel	2.6	60	241.9	191.4	475.0
	G2P2-St	9	Steel	0.5	60	322.6	251.2	621.8
	G1P3-Br	12	Brass	2.6	173	241.9	221.7	505.3
	G1P3-Al	12	Aluminum	2.6	155	241.9	221.7	505.3
	G1P3-St	12	Steel	2.6	60	241.9	221.7	505.3
	G2P3-St	12	Steel	0.5	60	322.6	289.5	660.1

(a) Particle channel with d_p=6 mm (P1)

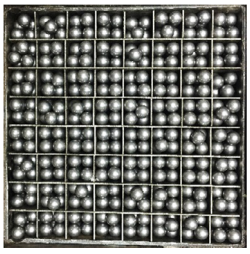

(b) Grille-particle channel with δ_g=0.5 mm and d_p=6 mm (G2P1)

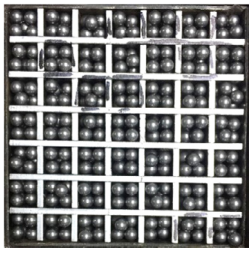

(c) Grille-particle channel with δ_g=2.6 mm and d_p=6 mm (G1P1)

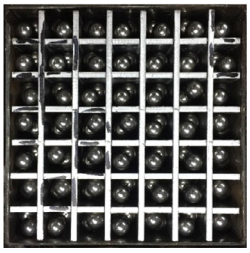

(d) Grille-particle channel with δ_g=2.6 mm and d_p=9 mm (G1P2)

(e) Grille-particle channel with δ_g=2.6 mm and d_p=12 mm (G1P3)

Fig. 3. Photos of a random particle channel and four grille-particle channels.

Table 2
Operating conditions for study.

Parameter	Value
Fluid flow rate	40–140 m^3/h
Re_p	224–3582
Re_D	7132–22238
Wall temperature	60–110 °C
Inlet air temperature	20–30 °C
Total heat flux	2–8 kW/m^2

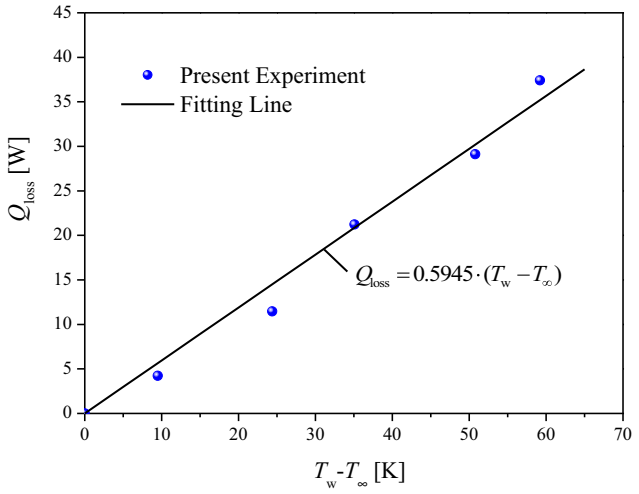

Fig. 4. Variation of heat loss with temperature difference between the channel wall and ambient.

$$T_{wx} = T_x - \frac{q_w \delta_w}{\lambda_w} \tag{6}$$

where q_w is heat flux of test channel, δ_w is distance from the bottom of a thermocouple groove to the inner surface of the test channel. T_w and T_f are then calculated according to

$$T_w = \sum_{i=1}^{11} \frac{T_{wx,i}}{11} \tag{7}$$

$$T_f = \frac{1}{2}(T_{in} + T_{out}) \tag{8}$$

2.4. Estimation of heat loss

As indicated earlier, heat loss in the present experiments is minimized by encasing the inlet channel, test channel and outlet channel with glass cotton fiber insulation. Nonetheless, some of the heat supplied by the electric film heater is eventually lost to the ambient. When all temperatures of the test channel's wall reach steady state, the total heat supplied by the film heater must equal the heat loss through the insulation. The following relation is used to relate the heat loss to temperature difference between the test channel's wall and ambient:

$$Q_{loss} = f(T_w, T_\infty) \tag{9}$$

To ascertain this functional dependence, various values of current (I) and voltage (V) are supplied to the film heater, and steady state temperatures of the channel wall (T_w) and ambient (T_∞) are recorded. This procedure provides the functional dependence of heat loss captured in Fig. 4 for each subsequent experiment.

2.5. Uncertainty analysis

The experimental uncertainty in determining the heat loss (Q_{loss}) is estimated at ±2%. The type-T thermocouples have an accuracy of ±0.2 °C. Pressures at the inlet and outlet are measured with the aid of pressure scanning valves having with full-scale range of 7 kPa and accuracy of ±0.05%. Accuracy of both vortex flowmeters is ±1.5%. Uncertainties in input current and input voltage measurements are ±1.0% and ±0.4%, respectively, and corresponding uncertainty in total heat input is ±1.08%. And uncertainties in calculated Reynolds number and Nusselt number according to the method by Moffat [25] are estimated at 5.4% and 6.9%, respectively.

3. Results and discussion

Experiments were initiated by first ensuring integrity and reliability of all components of the test facility. This was followed by measurement of pressure drop and heat transfer characteristics for the different grille-particle channels to assess the influences of sub-channel to particle diameter ratio, grille thermal conductivity and grill thickness. Finally, the performances of grille-particle channels were compared with those of random particle channels.

3.1. Validation of system reliability

Reliability of the experimental setup was validated by first measuring the fluid flow and heat transfer characteristics for random particle channels. For the validations, the channels were randomly filled with particles having diameters (d_p) of 6, 9, and 12 mm, and tube to particle diameter ratios (N) of 16.67, 11.11 and 8.33, respectively. The air flow rates ranged from 40 to 140 m^3/h, which correspond to particle Reynolds numbers (Re_p) from 224 to 3582. For the case of d_p = 6 mm (N = 16.67), tube to particle diameter ratio is relatively high, hence friction factors of the test channel were validated using Ergun's correlation [26] along with experimental data by Wang et al. [27] in which channel wall effects were relatively small. For the other two cases with d_p = 9 mm (N = 11.11) and d_p = 12 mm (N = 8.33), tube to particle diameter ratios are relatively small, and friction factors were validated using Eisfeld and Schnitzlein's correlation [28] in which channel wall effects were significant.

The friction factors for the validations were based on the following relations:

$$\begin{cases} f_v = \frac{\Delta p}{L}\frac{d_p^2}{\mu v_{in}}\frac{\varepsilon^3}{(1-\varepsilon)^2} = A + B\frac{Re_p}{1-\varepsilon} \\ A = A_W \cdot M^2, B = B_W \cdot M \\ M = 1 + \frac{2}{3(D/d_p)\cdot(1-\varepsilon)} \end{cases} \tag{10}$$

where $A_W = 150/M^2$ and $B_W = 1.75/M$ for the Ergun's correlation [26], and $A_W = 154$ and $B_W = \left[1.15/(D/d_p)^2 + 0.87\right]^{-2}$ for the Eisfeld and Schnitzlein's correlation [28].

Fig. 5 shows variations of friction factors for different random particle channels. For the case of d_p = 6 mm (N = 16.67), friction factors are shown agreeing quite well with Ergun's correlation [26] and Wang et al.'s experimental data [27]. Meanwhile, for d_p = 9 mm (N = 11.11) and d_p = 12 mm (N = 8.33), friction factors show good agreement with Eisfeld and Schnitzlein's correlation [28]. These results demonstrate the effectiveness of the present experimental setup at obtaining reliable pressure drop measurements for particle packed channels.

Further confirmation of the reliability of the experimental set up was achieved by validating measurements of average Nusselt number between heated channel wall and fluid with Yagi and Wakao's correlation [29],

$$Nu_{wf} = 0.2Pr^{1/3}Re_p^{0.8} \tag{11}$$

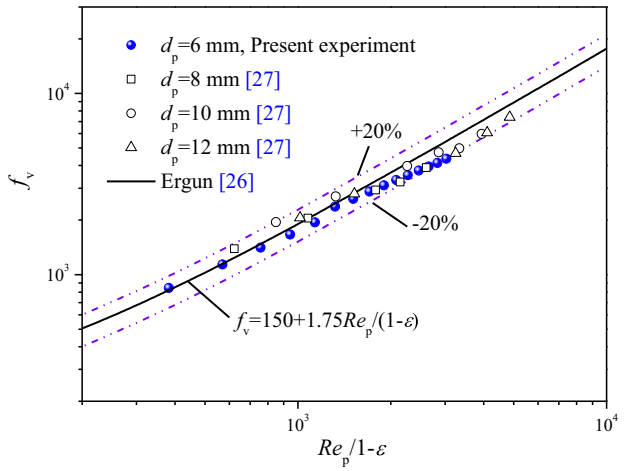

(a) d_p=6 mm

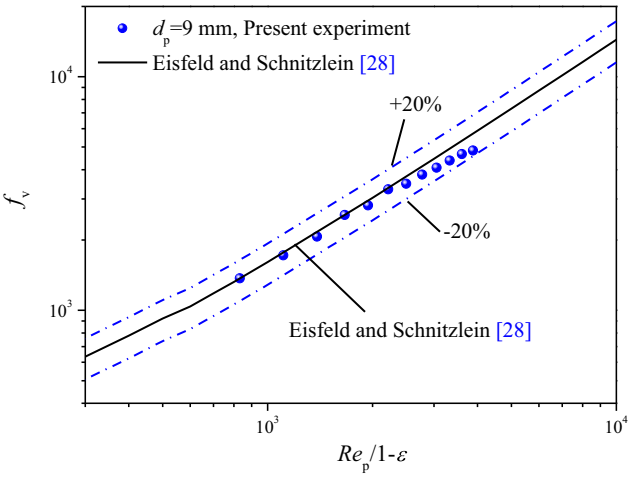

(b) d_p=9 mm

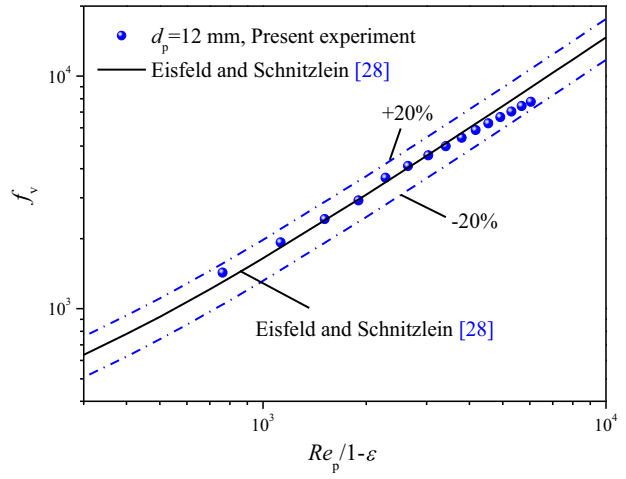

(c) d_p=12 mm

Fig. 5. Validations of friction factor in random particle channels.

Fig. 6 shows variations of measured Nusselt number for different random particle channels agree quite well with Yagi and Wakao's correlation [29], providing further evidence of the effectiveness and reliability of the present experimental setup.

3.2. Pressure drop and heat transfer performances in grille-particle composite packed bed

3.2.1. Effects of sub-channel to particle diameter ratio (N)

When investigating effects of sub-channel to particle diameter ratio, the same grille was used in the test channel. The grille is made of brass with a thickness of 2.6 mm, and contains an array of 7×7 sub-channels. Three different packings, with particle diameters of 6, 9 and 12 mm are used, which are designated as G1P1-Br (d_p = 6 mm), G1P2-Br (d_p = 9 mm) and G1P3-Br (d_p = 12 - mm) in Table 1. The packing structures of G1P1-Br, G1P2-Br and G1P3-Br can also be seen in Fig. 3(c), (d) and (e), respectively. Notice for d_p = 12 mm that sub-channel to particle diameter ratio (N) is unity, rendering packing structure in each sub-channel quite ordered, with the particles arranged in a linear fashion. While, for the other two configurations, with N = 1.3 (d_p = 9 mm) and N = 2.0 (d_p = 6 mm), packing structure in the individual sub-channels is less orderly. It should be noted that average porosities of sub-channels for N = 1.0, 1.3 and 2.0 are 0.48, 0.66 and 0.50, respectively.

Fig. 7 shows the variations of pressure drop and Nusselt number in grille-particle channels for different sub-channel to particle diameter ratios (N). For same Reynolds number, both pressure drop and Nusselt number are highest for N = 2.0 (d_p = 6 mm) and lowest for N = 1.3 (d_p = 9 mm). Notice also that higher porosity decreases pressure drop, hence pressure drop is noticeably smaller for N = 1.3 (d_p = 9 mm). Meanwhile, for the same porosity, smaller particle diameter tends to increase pressure drop because of higher surface area-to-volume ratio in the sub-channel. Therefore, pressure drop for N = 2.0 (d_p = 6 mm) is higher than that for N = 1.0 (d_p = 12 mm). As for heat transfer, higher surface area-to-volume ratio in the sub-channel culminates in better heat transfer performance. As shown in Table 1, total heat transfer area (A_{total}) is largest for N = 2.0 (d_p = 6 mm), which also corresponds highest surface area-to-volume ratio. Conversely, A_{total} is lowest for N = 1.3 (d_p = 9 mm). Therefore, Nusselt number is highest for N = 2.0 (d_p = 6 mm) and lowest for N = 1.3 (d_p = 9 mm).

Fig. 8 shows variations of overall heat transfer efficiency (γ) in the test channel for different sub-channel to particle diameter ratios (N). Here, the overall heat transfer efficiency (γ) is defined as

$$\gamma = \frac{h_{wf}}{\Delta p / L} \tag{12}$$

where h_{wf} is the heat transfer coefficient along the channel's hot wall (as defined in Eq. (3)), and $\Delta p/L$ the pressure drop in the test channel. From Fig. 8, the overall heat transfer efficiency is highest

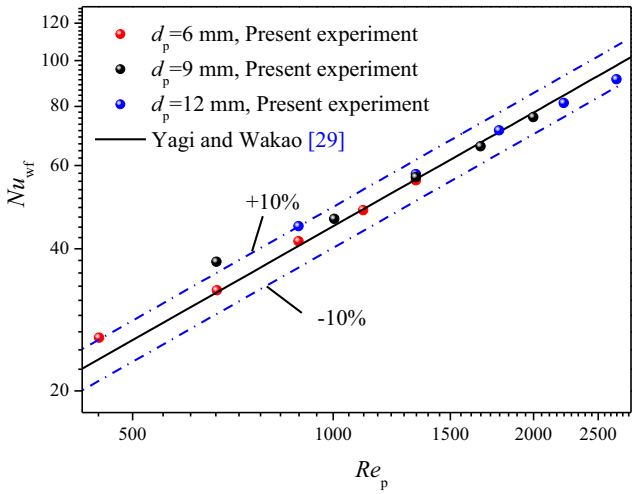

Fig. 6. Validations of Nusselt number in random particle channels.

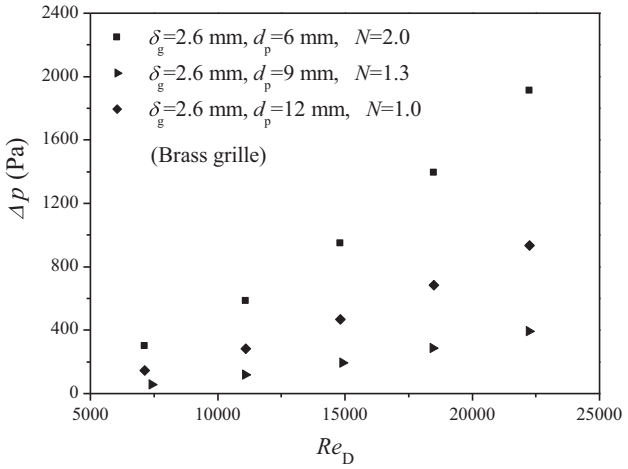

(a) Pressure drop

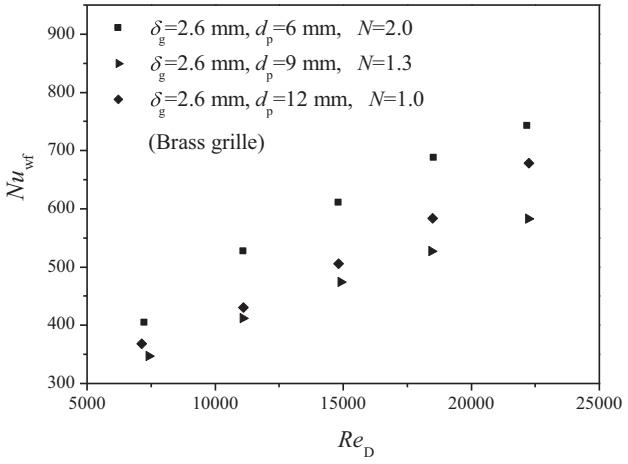

(b) Nusselt nubmer

Fig. 7. Variations of pressure drop and Nusselt number in grille-particle channels with different sub-channel to particle diameter ratios (*N*).

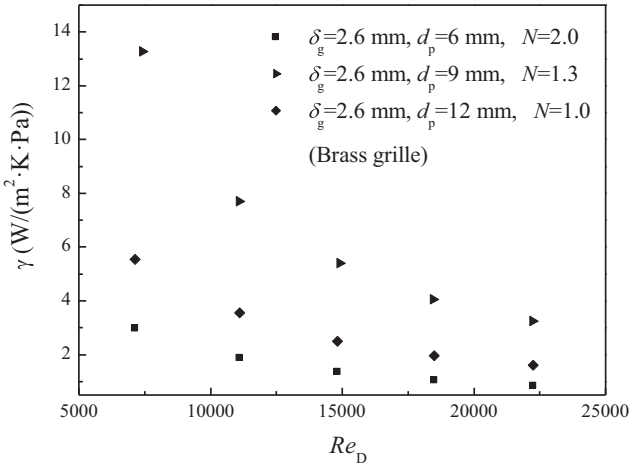

Fig. 8. Variations of overall heat transfer efficiency in grille-particle channels with different sub-channel to particle diameter ratios (*N*).

for $N = 1.3$ ($d_p = 9$ mm) and lowest for $N = 2.0$ ($d_p = 6$ mm). Therefore, GPCP packing, with its denser packing structure (say $N = 2.0$), improves heat transfer, albeit at the expense of increased pressure drop and reduced overall heat transfer efficiency. On the other hand, looser packing structure (say $N = 1.3$) weakens internal heat transfer, but both decreases pressure drop and increases overall heat transfer efficiency.

3.2.2. Effects of grille thermal conductivity

To investigate the effects of grille thermal conductivity, three different kinds of grille materials were tested, brass, aluminum and steel, with thermal conductivities of 173, 155 and 60 W/(m·K), respectively. However, a fixed grille thickness of 2.6 mm was used with all three grille materials. Since pressure drop in the test channel is insensitive to thermal conductivity of the grille, this portion of the study was focused mainly on heat transfer performance.

Fig. 9 shows variations of Nusselt number in grille-particle channels for different grille conductivities. For $N = 2.0$ ($d_p = 6$ mm) and $N = 1.3$ ($d_p = 9$ mm), higher conductivity is shown yielding higher Nusselt numbers. This trend can be explained by the higher conductivity improving heat transfer in the packed bed. On the other hand, $N = 1.0$ ($d_p = 12$ mm) is shown yielding similar Nusselt numbers for brass and aluminum, which are higher than those for steel. For $N = 1.0$ ($d_p = 12$ mm), each particle in the sub-channel is surrounded by, and in contact with four grille walls, so heat could be conducted more effectively from the grilles to the particles than with $N = 1.3$ ($d_p = 9$ mm) or $N = 2.0$ ($d_p = 6$ mm). For brass and aluminum grilles, the thermal conductivities are high enough, and the convection heat transfer would become a main constraint to the whole heat transfer rate, so the Nusselt numbers for the packings with brass grille and aluminum grille would be close to each other. As for the packing with steel grille, the grille thermal conductivity is relatively low, and the conduction heat transfer would become a main constraint to the whole heat transfer rate, therefore, the Nusselt numbers for the packing with steel grille would be lower.

Since pressure drop is insensitive to grille conductivity, variations of overall heat transfer efficiency for different grille materials are consistent with those of Nusselt number. Therefore, for packings with $N = 2.0$ ($d_p = 6$ mm) and $N = 1.3$ ($d_p = 9$ mm), higher grille conductivity would lead to higher overall heat transfer efficiency. On the other hand, for $N = 1.0$ ($d_p = 12$ mm), overall heat transfer efficiency would be fairly similar for brass and aluminum but lower for steel.

3.2.3. Effects of grille thickness

To investigate the effects of grille thickness on packed bed performance, the overall dimensions of the test channel were fixed. But, to maintain equal sub-channel dimensions, two different steel grilles with thickness of $\delta_g = 0.5$ mm and 2.6 mm were tested, resulting in 8×8 and 7×7 sub-channel arrays, respectively. Grille-particle structures for $\delta_g = 0.5$ mm ($d_p = 6$ mm) and $\delta_g = 2.6$ - mm ($d_p = 6$ mm) are depicted in Fig. 3(b) and (c).

Fig. 10 shows variations of pressure drop and Nusselt number in the grille-particle channels with different grille thicknesses. For same Reynolds number and particle diameter, pressure drop is higher for the thicker grille ($\delta_g = 2.6$ mm), while Nusselt numbers for the different grille thicknesses are close to one another. The pressure drop trends can be explained as follows. For same Reynolds number, sub-channel air velocity for $\delta_g = 2.6$ mm is higher than for $\delta_g = 0.5$ mm, therefore, the pressure drop is higher for $\delta_g = 2.6$ mm. Since sub-channels are arranged in parallel in the grille-particle channel, pressure drop for the entire channel is equal to that for a single sub-channel. Therefore, pressure drop for the thicker grille ($\delta_g = 2.6$ mm) should be higher. As for heat transfer, although air velocity in the sub-channel with thicker grille ($\delta_g = 2.6$ mm) is higher and thermal conduction resistance of the grille lower, total heat transfer area is about 20% smaller than with the thinner grille ($\delta_g = 0.5$ mm). As a result, the heat transfer per-

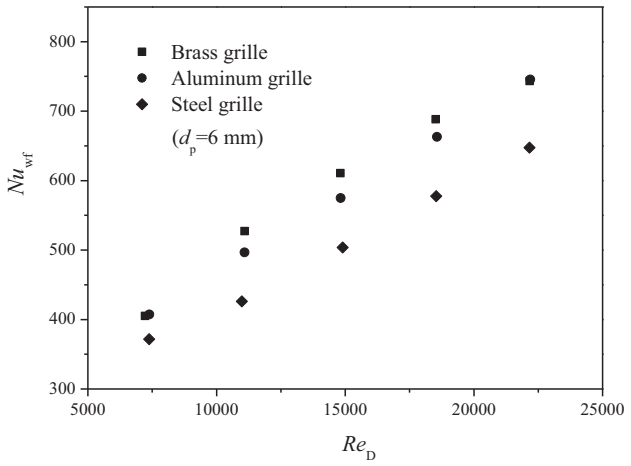

(a) d_p=6 mm

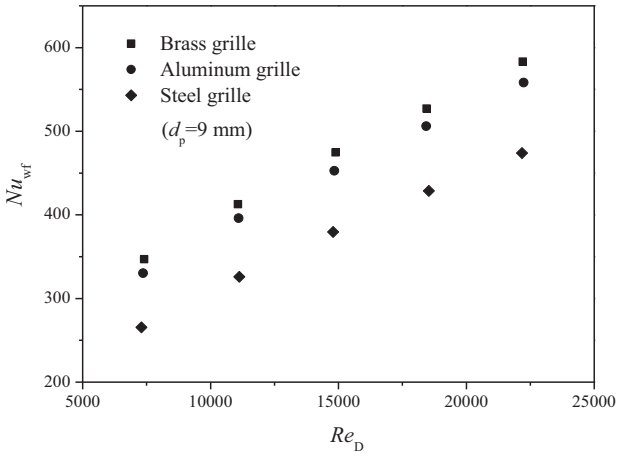

(b) d_p=9 mm

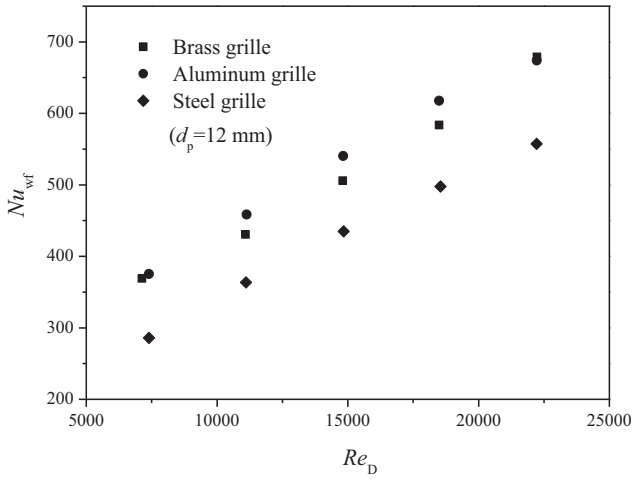

(c) d_p=12 mm

Fig. 9. Variations of Nusselt number in grille-particle channels with different grille thermal conductivities.

formance for packings with different grille thicknesses is somewhat similar. Taking both pressure drop and heat transfer into account, overall heat transfer efficiency for the grille-particle packing with thinner grille (δ_g = 0.5 mm) is therefore improved because of the lower pressure drop.

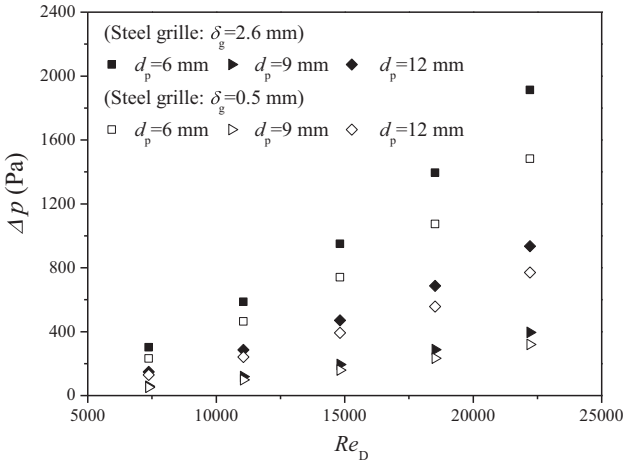

(a) Pressure drop

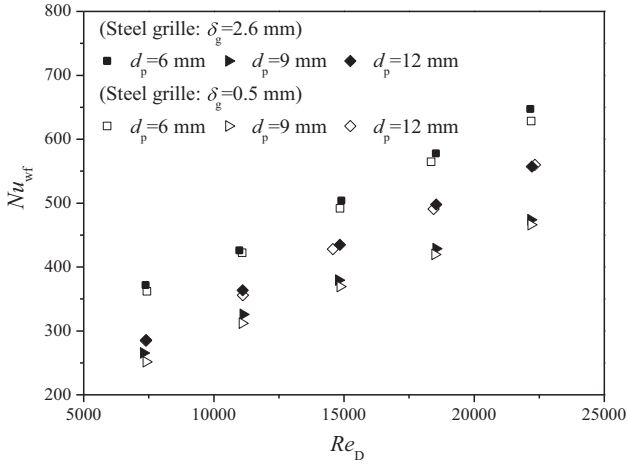

(b) Nusselt number

Fig. 10. Variations of pressure drop and Nusselt number in grille-particle channels with different grille thicknesses.

3.3. Performance comparison for random particle channel and grille-particle channel

It is now useful to compare pressure drop, Nusselt number and overall heat transfer efficiency of grille-particle channels to those of random particle channels. For the grille-particle channel, the comparison is based on the steel grille with 2.6 mm thickness. For the same particle diameter, this particular grille-particle channel was shown earlier to have the lowest overall heat transfer efficiency among all the grille-particle channels examined in the present paper. Geometrical and physical parameters for this comparison are provided in Table 1 for the grille-particle channels (G1P1-St, G1P2-St and G1P3-St), and Table 3 for the random particle channels (P1, P2 and P3).

Fig. 11 compares variations of pressure drop, Nusselt number and overall heat transfer efficiency for the grille-particle channel and random particle channel. Fig. 11(a) and (b) show both pressure drop and Nusselt number are higher for random particle channels than those for the grille-particle channels. This trend is the outcome of the grille forcing particles into a structured and ordered flow arrangement with increased porosity, which reduces pressure drop for the grille-particle channel. Additionally, reduced flow tortuosity and disturbance compromises heat transfer for the grille-particle channel. However, Fig. 11(c) shows that, for same Reynolds number and particle diameter, the overall heat transfer efficiency

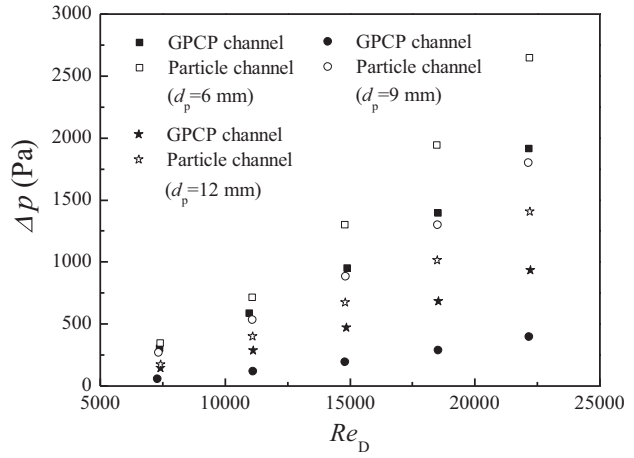

(a) Pressure drop

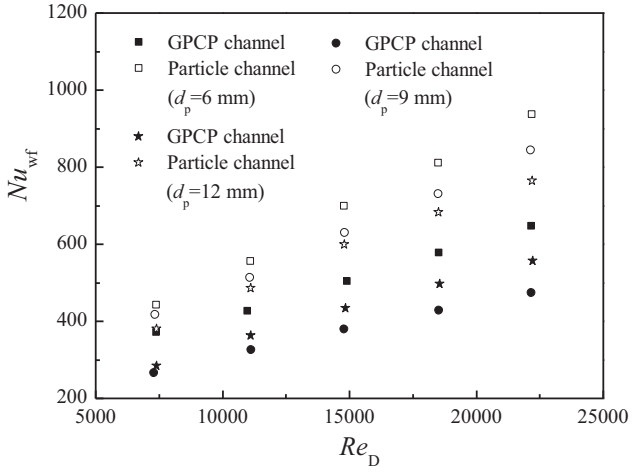

(b) Nusselt number

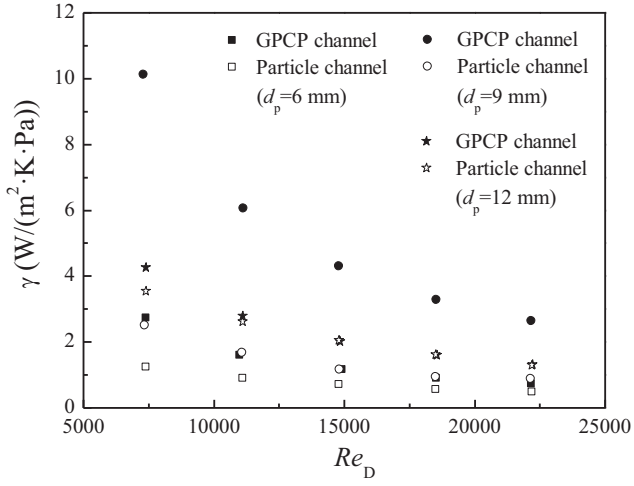

(c) Overall heat trasnfer coefficient

Fig. 11. Variations of pressure drop, Nusselt number and overall heat transfer efficiency in random particle channels and grille-particle channels.

(γ) is higher for grille-particle channel, especial for d_p = 6 mm and d_p = 9 mm. Notice that the overall heat transfer efficiency (γ) for the grille-particle channel with d_p = 6 mm, d_p = 9 mm and d_p = 12 - mm are improved, on average, by 73.46%, 255.70% and 4.88%, respectively. This would indicate that, for same channel size and particle diameter, the grille-particle channel provides superior overall heat transfer performance, especially for relatively small particle diameters. Furthermore, with proper selection of grille thermal conductivity, grille thickness and sub-channel to particle diameter ratio, the overall heat transfer efficiency for the grille-particle channel could be further improved. These results provide useful guidelines for the design of GPCP.

Table 3
Geometrical parameters for random particle channels.

Packings	d_p [mm]	N_p [–]	V_p [$\times 10^6$ m^3]	A_p [m^2]	N [–]	ε [–]
P1	6	6460	730.6	0.731	16.67	0.391
P2	9	1886	719.9	0.480	11.11	0.400
P3	12	786	711.2	0.356	8.33	0.407

4. Conclusions

This study provided a comprehensive experimental investigation of forced convection in grille-particle composite packed beds (GPCP). The effects of sub-channel to particle diameter ratio, grille thickness and grille thermal conductivity on pressure drop, Nusselt number and overall heat transfer efficiency were carefully analyzed for a grille-particle channel. And performances of grille-particle channels were also compared with those of random particle channels. The main conclusions from the study are as follows:

(1) Regarding effects of sub-channel to particle diameter ratio, it is found that denser packing (e.g., N = 2.0) enhances heat transfer in the grille-particle channel at the expense of higher pressure drop and reduced overall heat transfer efficiency. Conversely, looser packing (e.g., N = 1.3) weakens heat transfer in the grille-particle channel but decreases pressure drop and improves overall heat transfer efficiency.
(2) As for the effects of grille thermal conductivity, it is found that, for packings with N = 2.0 (d_p = 6 mm) and N = 1.3 (d_p = 9 mm), higher grille thermal conductivity increases Nusselt Number and overall heat transfer efficiency. While for packings with N = 1.0 (d_p = 12 mm), both Nusselt number and overall heat transfer efficiency are very similar for the brass grille and aluminum grille, but higher than those for the steel grille.
(3) In regards to grille thickness effects, it is found that, for same Reynolds number and particle diameter, thicker grille (δ_g = 2.6 mm) increases pressure drop but has only minor influence on Nusselt number. As a result, thinner grille (δ_g = 0.5 mm) provides superior overall heat transfer efficiency.
(4) When compared with random packings, for same channel size and particle diameter, heat transfer in the grille-particle channel is relatively weaker, but pressure drop is reduced and overall heat transfer efficiency improved. Compared to random particle channels, the overall heat transfer efficiency for the grille-particle channel with d_p = 6 mm, d_p = 9 mm and d_p = 12 mm are improved, on average, by 73.46%, 255.70% and 4.88%, respectively.

Conflict of interest

None.

Acknowledgements

The authors would like to acknowledge financial supports for this work provided by National Natural Science Foundation of China (No. 51476124, 51721004) and CSC Fellowship (No. 201806285048).

References

[1] P. Smakulski, S. Pietrowicz, A review of the capabilities of high heat flux removal by porous materials, microchannels and spray cooling techniques, Appl. Therm. Eng. 104 (2016) 636–646.
[2] D.A. Nield, A. Bejan, Convection in Porous Media, fourth ed., Springer, New York, Ch, 2013.
[3] Z.I. Önsan, A.K. Avci, Multiphase Catalytic Reactors: Theory, Design, Manufacturing, and Applications, John Wiley & Sons, Inc., 2016.
[4] M. Behnam, A.G. Dixon, 3D CFD simulations of local carbon formation in steam methane reforming catalyst particles, Int. J. Chem. Reactor Eng. 67 (2017) 1–17.
[5] A.S. Silva, L.Y. Rojas, D.S. Dominguez, C.R. Garcia, A. Gamez, A. Brayner, Realistic CFD simulation of HTR-10 reactor using a face centred cubic column, Int. J. Nucl. Energy Sci. Technol. 10 (2016) 217–233.
[6] T.M. Jeng, S.C. Tzeng, Q.Y. Huang, Heat transfer performance of the pin-fin heat sink filled with packed brass beads under a vertical oncoming flow, Int. J. Heat Mass Transf. 86 (2015) 531–541.
[7] P.X. Jiang, Z. Wang, Z.P. Ren, B.X. Wang, Experimental research of fluid flow and convection heat transfer in plate channels filled with glass or metallic particles, Exp. Therm Fluid Sci. 20 (1999) 45–54.
[8] P.X. Jiang, M. Li, T.J. Lu, L. Yu, Z.P. Ren, Experimental research on convection heat transfer in sintered porous plate channels, Int. J. Heat Mass Transf. 47 (2004) 2085–2096.
[9] T.M. Jeng, S.C. Tzeng, Y.C. Chen, Thermal characteristics in asymmetrically heated channels fully filled brass beads, Int. J. Therm. Sci. 50 (2011) 1853–1860.
[10] A.H. Ahmadi Motlagh, S.H. Hashemabadi, 3D CFD simulation and experimental validation of particle-to-fluid heat transfer in a randomly packed bed of cylindrical particles, Int. Commun. Heat Mass Transfer 35 (2008) 1183–1189.
[11] A.G. Dixon, G. Walls, H. Stanness, M. Nijemeisland, E.H. Stitt, Experimental validation of high Reynolds number CFD simulations of heat transfer in a pilot-scale fixed bed tube, Chem. Eng. J. 200–202 (2012) 344–356.
[12] H. Freund, T. Zeiser, F. Huber, E. Klemm, G. Brenner, F. Durst, G. Emig, Numerical simulations of single phase reacting flows in randomly packed fixed-bed reactors and experimental validation, Chem. Eng. Sci. 58 (2003) 903–910.
[13] M. Nijemeisland, A.G. Dixon, CFD study of fluid flow and wall heat transfer in a fixed bed of spheres, AIChE J. 50 (2004) 906.
[14] M.J. Baker, G.R. Tabor, Computational analysis of transitional air flow through packed columns of spheres using the finite volume technique, Comput. Chem. Eng. 34 (2010) 878–885.
[15] T. Eppinger, K. Seidler, M. Kraume, DEM-CFD simulations of fixed bed reactors with small tube to particle diameter ratios, Chem. Eng. J. 166 (2011) 324–331.
[16] X.Y. Guo, R. Dai, Numerical simulation of flow and heat transfer in a random packed bed, Particuology 8 (2010) 293–299.
[17] J. Yang, Q.W. Wang, M. Zeng, A. Nakayama, Computational study of forced convective heat transfer in structured packed beds with spherical or ellipsoidal particles, Chem. Eng. Sci. 65 (2010) 726–738.
[18] J. Yang, Q.W. Wang, S.S. Bu, M. Zeng, Q.W. Wang, A. Nakayama, Experimental analysis of forced convective heat transfer in structured packed beds with spherical or ellipsoidal particles, Chem. Eng. Sci. 71 (2012) 126–137.
[19] M.H. Kim, H.S. Lim, W.J. Lee, Computational fluid dynamics assessment of the local hot core temperature in a pebble-bed type very temperature reactor, J. Eng. Gas Turbines Power 131 (2009) 012905.
[20] V.A. Strangio, F.M. Dautzenberg, H.P.A. Calis, A. Gupta, Fixed catalytic bed reactor, International Patent Application PCT/US99/06242, priority date 23 March 1998.
[21] H.P.A. Calis, J. Nijenhuis, B.C. Paikert, F.M. Dautzenberg, C.M. van den Bleek, CFD modelling and experimental validation of pressure drop and flow profile in a novel structured catalytic reactor packing, Chem. Eng. Sci. 56 (2001) 1713–1720.
[22] S.J.P. Romkes, F.M. Dautzenberg, C.M. van den Bleek, H.P.A. Calis, CFD modelling and experimental validation of particle-to-fluid mass and heat transfer in a packed bed at very low channel to particle diameter ratio, Chem. Eng. J. 96 (2003) 3–13.
[23] J.Y. Wang, J. Yang, Z.L. Cheng, Y. Liu, Y.T. Chen, Q.W. Wang, Experimental and numerical study on pressure drop and heat transfer performance of grille-sphere composite structured packed bed, Appl. Energy (2018), https://doi.org/10.1016/j.apenergy.2017.07.140.
[24] Y.X. Hu, J. Yang, J.Y. Wang, Q.W. Wang, Investigation of hydrodynamic and heat transfer performances in grille-sphere composite pebble beds with DEM-CFD-Taguchi method, Energy 155 (2018) 909–920.
[25] R.J. Moffat, Contributions to the theory of single-sample uncertainty analysis, J. Fluids Eng. 104 (1986) 250–260.
[26] S. Ergun, Fluid flow through packed columns, Chem. Eng. Prog. 48 (1952) 89–94.
[27] J.Y. Wang, Y. Liu, J. Yang, T.Y. Chen, Q.W. Wang, Experimental investigation of axial heat transfer and entrance effect in randomly packed beds with naphthalene sublimation technique, Heat Transfer Res. 49 (2018) 235–253.
[28] B. Eisfeld, K. Schnitzlein, The influence of confining walls on the pressure drop in packed beds, Chem. Eng. Sci. 56 (2001) 4321–4329.
[29] S. Yagi, N. Wakao, Heat and mass transfer from wall to fluid in packed beds, AIChE J. 5 (1959) 79–85.